

---

---

GENERAL EXPERIMENTAL  
TECHNIQUE

---

---

## MK-200 Plasma Gun Facility

V. A. Kostyushin<sup>a,\*</sup>, I. M. Poznyak<sup>a,b</sup>, D. A. Toporkov<sup>a,b</sup>, D. A. Burmistrov<sup>a,c</sup>, K. V. Zhuravlev<sup>a</sup>,  
S. D. Lidzhigoryaev<sup>a,b</sup>, R. R. Usmanov<sup>a,c</sup>, V. Yu. Tsybenko<sup>a</sup>, and V. S. Nemchinov<sup>a</sup>

<sup>a</sup>State Scientific Center of the Russian Federation Troitsk Institute for Innovation and Fusion Research,  
Moscow, 108840 Russia

<sup>b</sup>Moscow Institute of Physics and Technology (National Research University),  
Dolgoprudny, Moscow oblast, 141701 Russia

<sup>c</sup>National Research University Moscow Power Engineering Institute,  
Moscow, 111250 Russia

\*e-mail: vakostyushin@triniti.ru

Received December 8, 2022; revised April 6, 2023; accepted April 8, 2023

**Abstract**—Plasma flows with high velocity, density, and energy are widely used in research on the interaction of plasma with materials, modeling of astrophysical processes, development of plasma thrusters and plasma radiation sources, and plasma injection into fusion devices. Electrodynamical plasma guns can be used to generate such flows. This paper describes the design features of a powerful pulsed plasma gun and diagnostic tools for measuring the parameters of the plasma flow generated by it.

DOI: 10.1134/S0020441223050111

### INTRODUCTION

Plasma flows with high velocity, density, and energy are widely used in solving various research and technological problems. Such problems include interaction of plasma with materials [1], modeling of astrophysical processes [2], development of plasma thrusters [3, 4] and plasma radiation sources [5], and plasma injection into fusion devices [6]. Powerful plasma flows can be generated using electrodynamic plasma guns.

When deuterium or tritium is used as a plasma-forming gas, the generation of thermonuclear neutrons is possible in the case of an oncoming collision of plasma flows. The energy of the relative motion of interacting particles is four times higher than their kinetic energy, so the intensity of neutron radiation from the collision zone will be at least four times higher than the intensity of neutron radiation from a plasma cloud with a Maxwellian ion energy distribution for the same values of energy content, plasma mass, and density [7]. This makes it possible to create a powerful source of thermonuclear neutrons based on pulsed plasma guns.

### INSTALLATION DESCRIPTION

The layout of the MK-200 facility with diagnostic equipment is shown in Fig. 1. The facility consists of an electrodynamic pulsed plasma gun, a cylindrical chamber for transporting the plasma flow, and a target chamber. The transportation chamber is a cylindrical

300-cm-long stainless-steel pipe, with an inner diameter of 20 cm and a wall thickness of 3 mm, in which a quasi-stationary longitudinal magnetic field is created using multiturn solenoids. The inner diameter of the plasma duct is 4 cm larger than the output diameter of the outer electrode of the gun, which ensures the presence of a magnetic gap between the plasma and the chamber wall. A target chamber in the form of a cylindrical stainless-steel tube with a diameter of 29 cm and a length of 42 cm is attached to the transportation chamber, into which test samples or diagnostic equipment (calorimeter for measuring the total energy content of the plasma flow, pressure sensors, etc.) can be installed. During the experiment, a longitudinal magnetic field is created in the target chamber using Helmholtz coils.

The electrode system of the plasma gun (PA) is made in the form of two truncated coaxial copper cones. The outer electrode (anode) is not solid but is made up of 18 individual rods, which prevents the discharge current from being “laced.” The diameter of the outer electrode at the base is 220 mm and it is 170 mm at the exit from the gun. The diameter of the inner electrode (cathode) varies in length from 120 to 43 mm. The length of the electrodes on which the plasma sheath is accelerated is ~490 mm. At the base, the electrodes are separated by a polyacetal insulator, located in such a way as to exclude the direct effect of the discharge light radiation on the insulator to prevent the development of secondary breakdowns along its surface.

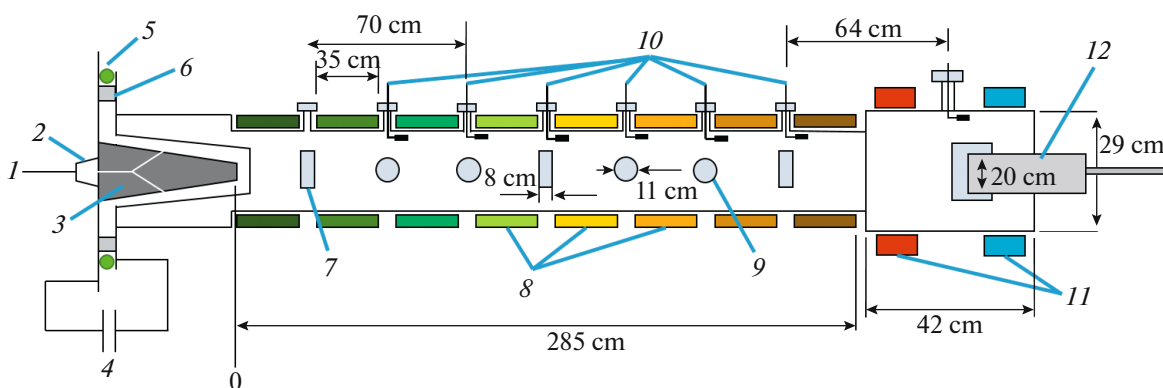


**Fig. 1.** Scheme of the MK-200 installation. (1) Gas line; (2) gas valve; (3) plasma accelerator; (4) capacitor bank; (5) Rogowski coil; (6) insulator; (7) rectangular diagnostic windows; (8) magnetic field coils; (9) round diagnostic windows; (10) magnetic probes; (11) Helmholtz coils; (12) calorimeter.

The plasma gun is powered by a low-inductance capacitor bank consisting of 350 IK-50-3 capacitors with a total capacity of  $\sim 1.08$  mF. The battery charge voltage varies in the range of 14–24 kV, which corresponds to a change in the energy stored in the battery from 98 to 288 kJ. To switch the battery to the accelerator electrodes, eight disk vacuum dischargers are used. The arresters are connected to the electrode flanges with the help of 216 RK 50-11-13 coaxial cables to reduce the “stray” inductance of the discharge circuit and prevent current “lacing” between the gun electrodes.

The inlet of the working gas (hydrogen, deuterium, or nitrogen) into the interelectrode gap of the gun is carried out using a quick-acting valve. From a mechanical point of view, the valve is of the poppet type, i.e., the gap through which the gas passes is opened by a plate. The plate is a disk, the periphery of which, when closed, fits snugly against the seal. To open the annular gap, the poppet is pushed away from the seal. The shift of the plate is carried out due to the rectilinear movement of the rod, which simultaneously performs the function of a guide and a link connecting the plate with the actuator.

For valves of plasma accelerators, the inductive-dynamic type of the actuator is used. It is based on a flat electromagnetic coil, which is closely adjacent to a flat pusher made of electrically conductive material. When a current pulse is passed through the coil, eddy (induction) currents arise in the pusher material. Due to the short duration of the current pulse, the field is concentrated in the gap between the coil and the pusher, so they are affected by significant ponderomotive forces, which throw the pusher away from the coil. Through the stem, the movement of the pusher is transmitted to the valve disc. The valve is powered through a high-voltage isolating transformer, which provides electrical decoupling between the capacitor banks, from which the valve is powered, and the plasma gun.

Plasma motion from the gun to the target chamber occurs along a plasma pipeline filled with a longitudinal magnetic field. The magnetic field in the plasma duct is generated by eight multiturn solenoids and in the target chamber by Helmholtz coils. The solenoids and coils are powered by independent capacitor banks, which makes it possible to vary the field strength along the length of the plasma duct and in the target chamber. Each battery consists of 215 K-41I-7 capacitors (100  $\mu$ F, 5 kV) with a total capacity of 21.5 mF. Switching of batteries to coils is carried out with the help of disk vacuum arresters. The period of the discharge current in the solenoids lies in the range  $T = 8$ –18 ms. The magnitude of the generated magnetic field can vary in the range from 0 to 2 T.

Magnetic field distribution  $B(z)$  along the plasma pipeline is measured using a line of eight magnetic probes. Probes are cylindrical coils on a dielectric rod with a diameter of 20 mm, containing 25 turns of PELShO wire wound close to each other. The distance between adjacent probes in the line is 10 cm. Calibration of the probes is carried out according to the signal of the probe of a known section. According to the calibration results, the area of the probes lies in the range from 80 to 90 cm<sup>2</sup>.

The battery of each coil is energized  $U_i = 1$  kV for several starts; moving the array of probes along the plasma pipeline, the distribution is measured  $B(z)$ . Since the field of the solenoid  $B$  is proportional to the current flowing through it  $I$ , the maximum of which is proportional to the initial voltage  $U$  of the capacitor bank discharged onto it, then, according to the measurement results, the coupling coefficients  $k_i$  were calculated from the following expression:

$$B(z) = \sum_{i=1}^{10} k_i U_i$$

Knowing the coefficients  $k_i$ , one can calculate the voltages  $U_i$  to which each battery needs to be charged

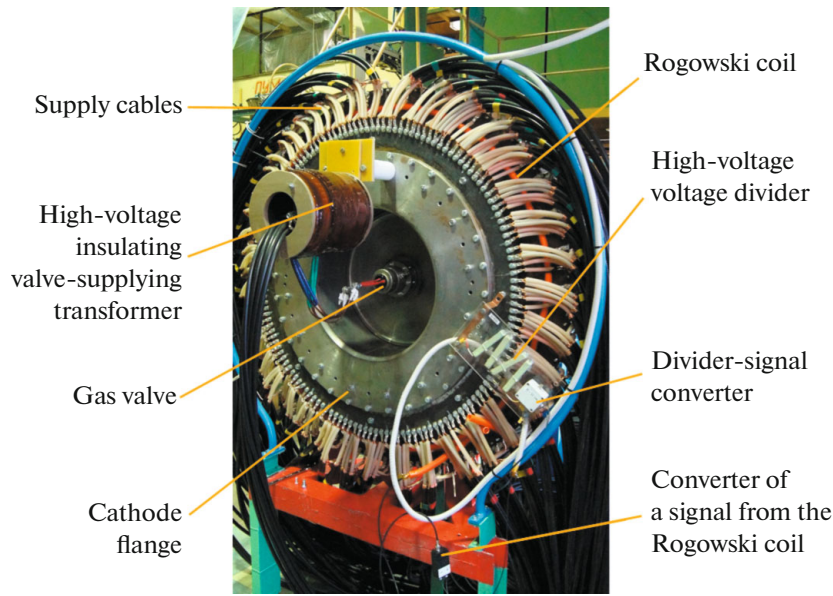


Fig. 2. Appearance of a high-voltage voltage divider, Rogowski coil, and signal converters.

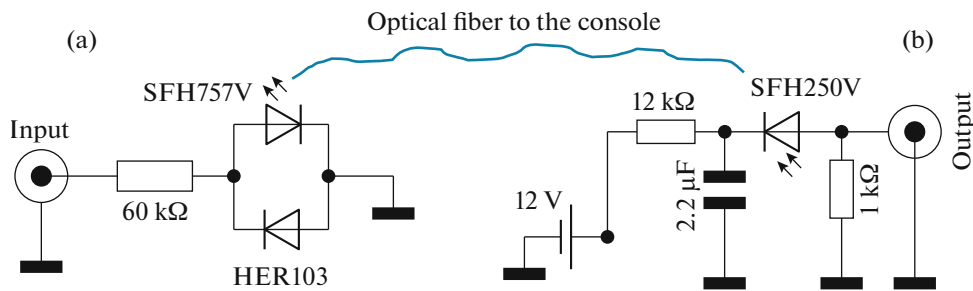


Fig. 3. Scheme for measuring the voltage on the gun electrodes: (a) high-voltage electro-optical converter; (b) photoelectric converter.

to obtain the required distribution during the experiment  $B(z)$ .

### DIAGNOSTIC TOOLS

To control the operating modes of the plasma gun and measure the parameters of the plasma flow, a number of diagnostic tools were created: a Rogowski coil, a high-voltage divider, magnetic probes, and an integral thermocouple calorimeter.

Optical decoupling was used to reduce the effect of electromagnetic pickups arising during the operation of the installation on the results of current and voltage measurements. Voltage  $U$  on the electrodes of the gun was recorded using a high-voltage electro-optical converter, a general view of which is shown in Fig. 2. The converter consists of low-inductance TVL-type resistors in the upper arm and a high-speed SFH757V LED in the lower arm (Fig. 3a). The resistance of the upper arm is  $\approx 60 \text{ k}\Omega$  and, at a voltage  $U = 20 \text{ kV}$ , limits the current through the LED to  $1/3 \text{ A}$ , which ensures its

operation in a linear mode. Voltage reversal protection is provided by shunting the SFH757V with a HER103 semiconductor diode connected in the opposite direction.

The LED signal is transmitted through an optical fiber and enters a photoelectric converter, the circuit of which is shown in Fig. 3b. The buffer capacitance of  $2.2 \mu\text{F}$  is charged to the power supply voltage of  $12 \text{ V}$  through a  $20 \text{ k}\Omega$  resistor. The SFH250V photodiode is opened by a light signal from the optical line, which leads to the flow of current through a  $1 \text{ k}\Omega$  resistor, the voltage across which is recorded by a TiePie HS4-50 digital oscilloscope. With a plasma discharge duration of no more than  $30 \mu\text{s}$  and the full opening of the photodiode, the capacitance of the buffer capacitor provides a reverse bias voltage drop of no more than  $0.16 \text{ V}$  (at a total signal amplitude of  $12 \text{ V}$ ).

The voltage divider is calibrated by applying a known DC voltage  $U$  to the gun electrodes. During calibration, the plasma gas is not supplied to the gun.

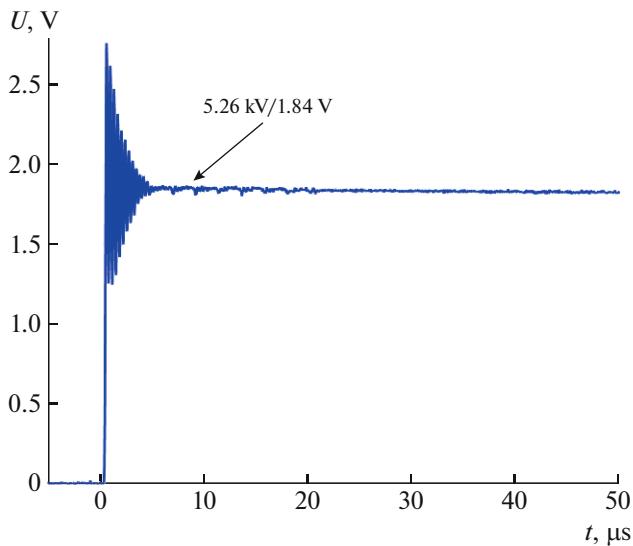


Fig. 4. Voltage divider signal during calibration.

When a capacitor bank is switched to the gun electrodes in a coaxial line (current-carrying cables), oscillations occur, the decay rate of which depends on the active resistance of the circuit. Such fluctuations are also preserved during the operating start-ups of the installation; however, they do not interfere with voltage measurements at the gun.

The signal received at  $U = 5.26$  kV is shown in Fig. 4. It can be seen that the oscillations decay in  $\approx 5$   $\mu$ s, and the response of the measuring channel is 1.84 V; the sensitivity factor of the divider is 2.86 kV/V.

To measure the discharge current  $I$ , a Rogowski coil was made. The belt is a core of a coaxial cable brand RG-58 with a diameter of 0.8 mm, on the polyethylene insulation of which a thin copper wire is wound with a pitch of 5 mm  $\varnothing$  0.2 mm in lacquered insulation. To protect against mechanical damage and electrical breakdowns, the coil is placed in a heat-shrinkable tube and polyethylene corrugation. The corrugation is laid between the gun busbars so that the Rogowski coil measures the entire discharge current (Fig. 2). The conversion, transmission, and registration of the signal from the coil was carried out according to the scheme with optical decoupling. The main difference from the circuit used with a voltage divider is the presence of two channels: both for the positive and for the negative component of the signal. The signal from the Rogowski coil is proportional to the derivative of the current, and the real value of the current is restored by a numerical method.

A typical signal from the Rogowski coil during the start-up of the MK-200 facility is shown in Fig. 5. Curves correspond to positive ( $+dI/dt$ ) and negative ( $-dI/dt$ ) components of the current derivative.

Figure 6 shows typical oscillograms with real values of current and voltage. In the given start-up, the voltage on the capacitor bank is 18 kV, the gas puff time before applying voltage to the electrodes is 270  $\mu$ s, and the working gas is deuterium.

One of the most common methods for measuring pulsed magnetic fields is the method based on the use of magnetic probes. For this setup, probes were made in the form of cylindrical coils 25 mm long and 3 mm in diameter. The coils contain 250 turns of 100  $\mu$ m thick copper wire wound close to each other. To ensure

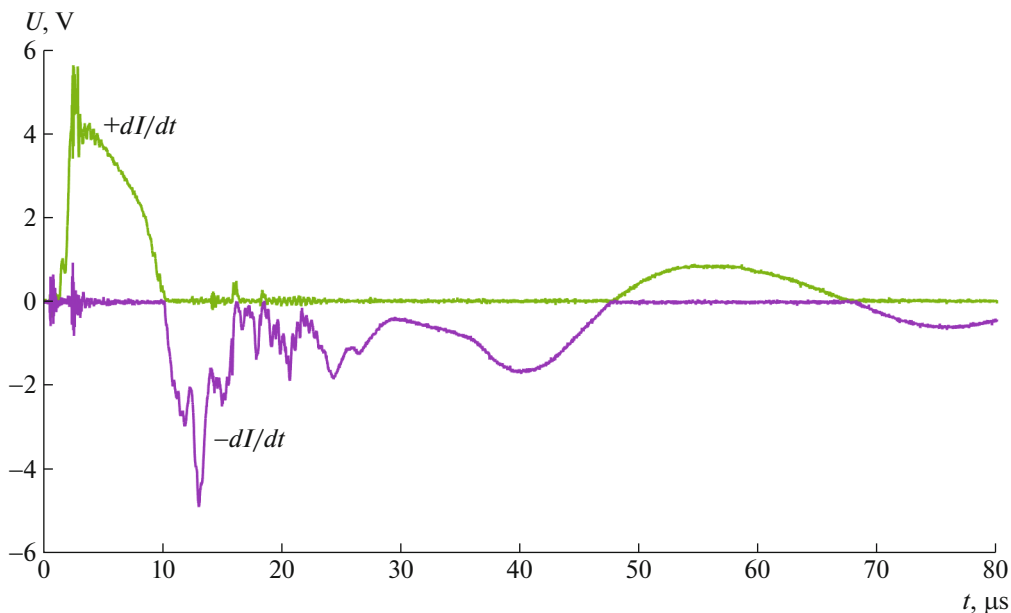


Fig. 5. Signal from the Rogowski belt.

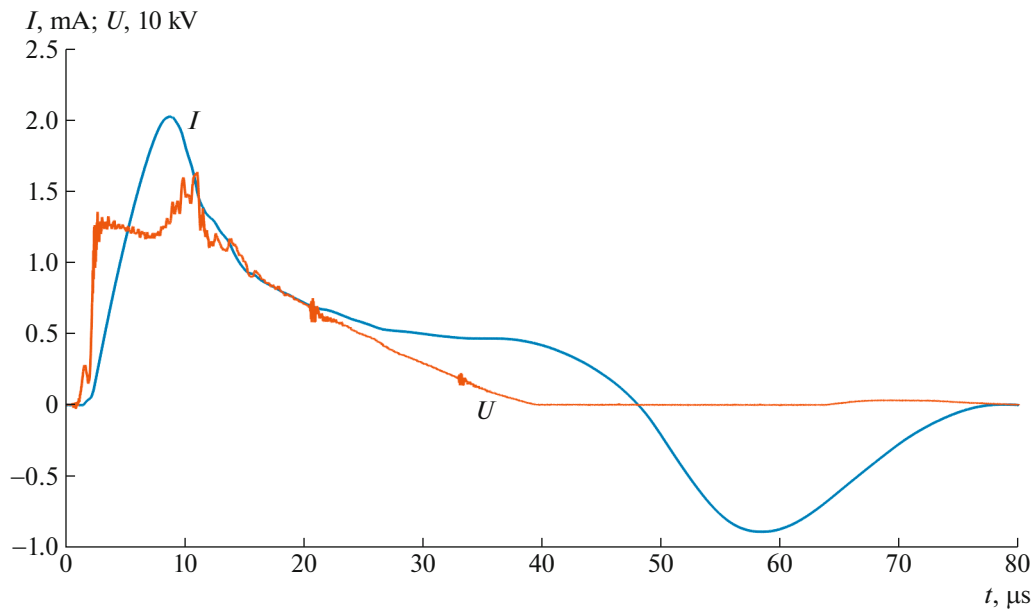


Fig. 6. Oscillograms of current and voltage.

the isolation of the coils from the plasma, they are placed in a ceramic case and sealed with epoxy resin. The probes are installed along the plasma pipeline at a distance of 35 cm from each other through a special vacuum seal, which makes it possible to isolate the probe body from the wall of the vacuum chamber and change its position (along the chamber radius) without violating the tightness of the installation.

When a probe with a total area of turns  $S$  is placed in an alternating magnetic field  $\mathbf{H}$ , induced at the ends of the coil EMF,  $U(t)$  is equal to the following:  $U(t) =$

$$S\mu_0 \frac{dH}{dt}.$$

The magnitude of the induction of the magnetic field  $B \sim \int U(t) dt$ . In the experiment, the integration of the signal is carried out using passive  $RC$ -chains. The time constant of the chains is  $200 \mu\text{s}$ , which satisfies the requirement  $RC \gg t_{\text{pl}}$ , where  $t_{\text{pl}}$  is the plasma flow duration ( $t \approx 30 \mu\text{s}$ ). Calibration of probes (determination of area  $S$ ) was carried out according to the known value of the magnetic field created using a long solenoid, on the winding of which a capacitor bank is discharged.

Based on the results of probe measurements, one can determine the plasma flow velocity  $V_{\text{pl}}$ , its duration  $t_{\text{pl}}$  and cross-sectional area  $S_{\text{pl}}$ . Plasma flow duration  $t_{\text{pl}}$  is determined at each start of the installation. To do this, the duration of the readings of the probes is measured at a level of 50% of the maximum value of the probe signal (Fig. 7). Plasma bunch speed  $V_{\text{pl}}$  can be estimated using the time-of-flight technique, knowing the distance between the magnetic probes  $L$  and measuring the delay of their signals  $\Delta t$ .

When moving along the plasma pipeline, the plasma bunch displaces the magnetic field to the walls of the vacuum chamber; however, the magnetic field does not have time to diffuse through the wall during the characteristic time of plasma movement. Thus, by the increment of the magnetic field  $\Delta B$ , measured by near-wall magnetic probes, and based on the law of conservation of the magnetic flux in the cross section of the plasma pipeline, it is possible to determine the area of the plasma flux:  $S_{\text{pl}} = \Delta BS / (B_0 - B_{\text{pl}} + \Delta B)$ , where  $S$  is the cross-sectional area of the plasma pipeline,  $B_0$  is the value of the initial magnetic field in the plasma duct, and  $B_{\text{pl}}$  is the value of the magnetic field in the area occupied by the plasma, which is measured using a magnetic probe lowered into the center of the plasma pipeline.

An integral calorimeter was made to measure the energy content of the plasma flow. The design of the calorimeter ensures uniform distribution of plasma flow energy by its inner surface, which increases the accuracy of measurements and increases the service life of the calorimeter. The wall temperature is measured using 16 chromel–alumel thermocouples fixed on the outer surface of the device. The thermocouples were calibrated using a thermostat.

Thermocouple signals are fed to industrial modules AIN8-U60 [8]. Each module has eight galvanically isolated (2.5 kV) inputs, the signal from which is amplified and then multiplexed to an 8-channel ADC. Data from the ADC is automatically transferred to a personal computer and stored in the database. To process the measurement results, a special program was written, which was used to interpolate data on the temperature increase of the calorimeter walls after plasma



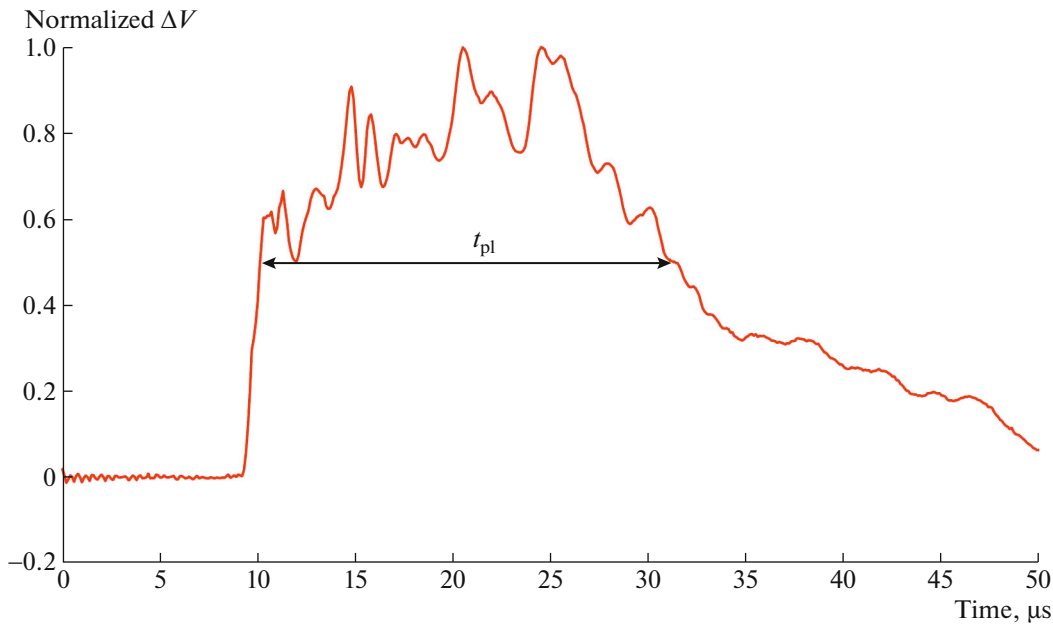


Fig. 7. Determining the plasma flow duration according to the signal of near-wall magnetic probe no. 2.

exposure, followed by the calculation of the total energy content of the plasma flow.

## CONCLUSIONS

In the presented work, the design features of a powerful pulsed plasma gun are described, diagnostic tools for measuring the parameters of the plasma flow generated by it are presented, and methods for processing experimental data are proposed. In the future, it is planned to supplement the diagnostic complex of the facility with a Mach–Zehnder interferometer for measuring the plasma flux density and to study the operating modes of the plasma gun.

## FUNDING

The work was carried out under the state contract no. H.4k.241.09.22.1074 dated April 28, 2022.

## OPEN ACCESS

This article is licensed under a Creative Commons Attribution 4.0 International License, which permits use, sharing, adaptation, distribution and reproduction in any medium or format, as long as you give appropriate credit to the original author(s) and the source, provide a link to the Creative Commons license, and indicate if changes were made. The images or other third party material in this article are included in the article's Creative Commons license, unless indicated otherwise in a credit line to the material. If material is not included in the article's Creative

Commons license and your intended use is not permitted by statutory regulation or exceeds the permitted use, you will need to obtain permission directly from the copyright holder. To view a copy of this license, visit <http://creativecommons.org/licenses/by/4.0/>.

## REFERENCES

1. Poznyak, I.M., Arkhipov, N.I., Karelov, S.V., Safronov, V.M., and Toporkov, D.A., *Vopr. At. Nauki Tekh., Ser.: Termoyad. Sint.*, 2014, vol. 37, no. 1, p. 70. <https://doi.org/10.21517/0202-3822-2014-37-1-70-79>
2. Anan'ev, S.S., Krauz, V.I., Myalton, V.V., and Kharrasov, A.M., *Vopr. At. Nauki Tekh., Ser.: Termoyad. Sint.*, 2017, vol. 40, no. 1, p. 21. <https://doi.org/10.21517/0202-3822-2017-40-1-21-35>
3. Koval'chuk, M.V., Il'gisonis, V.I., and Kulygin, V.M., *Priroda* (Moscow, Russ. Fed.), 2017, no. 12, p. 33.
4. Zhil'tsov, V.A. and Kulygin, V.M., *Vopr. At. Nauki Tekh., Ser.: Termoyad. Sint.*, 2018, vol. 41, no. 3, p. 5. <https://doi.org/10.21517/0202-3822-2018-41-3-5-20>
5. Toporkov, D.A., Gavrilov, V.V., Zhitlukhin, A.M., Kochnev, D.M., Kostyushin, V.A., Poznyak, I.M., Prikuz, S.A., Ryazantsev, S.N., and Skobelev, I.Yu., *Proc. 47th EPS Conference on Plasma Physics, EPS 2021*, Sitges, 2021, p. 545.
6. Raman, R., *Fusion Eng. Des.*, 2008, vol. 83, nos. 10–12, p. 1368. <https://doi.org/10.1016/j.fusengdes.2008.06.043>
7. Starostin, A.N., Zhitlukhin, A.M., Petrushevich, Yu.V., Taran, M.D., Filippov, A.V., Fortov, V.E., and Cherkovets, V.E., *JETP Lett.*, 2019, vol. 110, no. 6, p. 405. <https://doi.org/10.1134/S0021364019180085>
8. AIN8-U60 Analog Input Module. <http://dep.ru/catalog/68/ain8-u60/>.